Computational Materials Science 230 (2023) 112455

Contents lists available at ScienceDirect

Computational Materials Science

journal homepage: www.elsevier.com/locate/commatsci

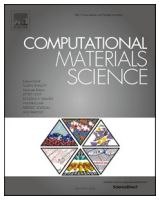

Full Length Article

Atomistic simulation of carbide formation in ferrite

R.J. Slooter [a,*], M.H.F. Sluiter [a], W.G.T. Kranendonk [b], C. Bos [a,b]

[a] Department of Materials Science and Engineering, Delft University of Technology, Mekelweg 2, 2628 CD Delft, The Netherlands
[b] Tata Steel, 1970 CA IJmuiden, The Netherlands

ARTICLE INFO

Keywords:
Carbides
Ferrite
MEAM
Precipitates

ABSTRACT

In this study possible routes from dissolved M and C atoms to a M-C (M = Ti, Nb) cluster are studied. Using atomistic modelling to perform relaxation simulations and molecular dynamics (MD) simulations for the Fe-M-C ternary system, the formation of clusters is studied for M. Additionally the stability of M-C clusters is assessed. The clustering of M and C atoms as observed in experiments is also found in simulations. The initial clusters found in this work have a (Fe,M)C composition with a large Fe fraction. Moreover, structurally relaxed clusters reveal that there are growth pathways with a monotone decrease in Gibbs energy, suggesting that the highest energy barrier in the formation of M-C clusters is the diffusion barrier for the atoms forming the cluster.

The development of M-C clusters as found in this study suggests a formation mechanism for nano-precipitation of carbides consisting of several steps; first a C cluster forms, then M atoms attach to the C cluster forming a (Fe,M)C cluster, and in the final step the (Fe,M)C cluster transforms to a NaCl-structured carbide.

1. Introduction

Predicting precipitate development in micro-alloyed steels is a key part in optimally utilizing the precipitation hardening effect. The number of precipitates and their size are determining factors in hardening, e.g., [1,2]. Understanding the formation of precipitates is therefore of critical importance. In transmission electron microscopy (TEM) and atom probe tomography (APT) it has been shown that various carbides initially form as platelets in the (1 0 0) planes of the bcc-Fe lattice [3–9], which can be linked to the Baker-Nutting interface orientation relation (BN-OR) [10]. The initial stoichiometry differs from the final stoichiometry of a metal carbide 'MC' (e.g. NbC, TiC, or VC) [4,6,11]. Additionally the shape changes over time [8], observes plate thickening, and [5] shows that a platelet grows into a lenticular shaped particle, but for larger precipitates a spheroidal form has been observed, e.g., [12].

These experiments have shown that the formation of carbides appears to occur in several steps. Wang et al. [6] distinguish an 'embryo-cluster', a 'Guinier-Preston (GP) cluster', and finally a NaCl-structured nano-precipitate. Both the embryo-cluster and GP-cluster are coherent with the bcc-ferrite matrix, in this work both will be referred to as 'proto-precipitate' as they are similar in appearance. The GP-zone clustering has also been observed for Nb-nitrides [4,7].

In this work the process leading up to the formation of such a proto-precipitate is investigated using static relaxation at 0 K and molecular dynamics (MD) at finite temperatures using Modified Embedded Atom Method (MEAM) potentials in the LAMMPS molecular dynamics simulation software [13]. First the pair interactions for several M-M, M-C and C-C atom pairs are calculated, here the results for the MEAM potentials are compared to Density Functional Theory (DFT) results. From static relaxation of larger clusters it is found that the formation of stable M-rich clusters is preceded by the formation of carbon clusters, or, at higher temperatures by the occurrence of carbon cluster fluctuations, next, on these carbon clusters the M atoms then attach to form a proto-precipitate with an ordered $FeMC_3$ structure observed for both Nb and Ti. The $FeMC_3$ clusters are estimated to be thermally stable at temperatures over 1100 K for $FeNbC_3$, and $FeTiC_3$ clusters are estimated to be stable at temperatures near the ferrite–austenite transition temperature of 1185 K. From these findings it can be derived that instead of a classical model for nucleation [14–17], the formation of M-carbides occurs in several steps; i) ordering of C atoms in Fe with local accumulation or clustering of C atoms, ii) attraction of M atoms and stabilisation in a $FeMC_3$ cluster, and iii) structural transformation to NaCl-structured nano-precipitate. The structural transformation is studied elsewhere [18].

First the methodology used to simulate various clusters is explained in Section 2. Then in Section 3 the results for various simulations are presented. In Section 4 the results are discussed.

* Corresponding author.
E-mail address: R.J.Slooter@tudelft.nl (R.J. Slooter).

https://doi.org/10.1016/j.commatsci.2023.112455
Received 10 March 2023; Received in revised form 31 July 2023; Accepted 21 August 2023
Available online 11 September 2023

2. Methodology

2.1. Static relaxations in Fe-M-C using LAMMPS

In order to simulate atom clusters a MEAM potential for the Fe-Nb-C [19] and Fe-Ti-C [20] ternary systems is used. LAMMPS (v 3mar20) [13] was used for static relaxations, MD, and Nudged Elastic Bands (NEB) method calculations. Stopping criteria are set such that the energy change between iterations is $1 \bullet 10^{-8}$ eV, and the magnitude of all force components on any atom must be less than $1 \bullet 10^{-8}$ eV/Å. Simulations are performed at constant volume, all supercells consist of a bcc lattice of $n \times n \times n$ bcc unit cells with a lattice parameter fixed at $n \bullet 2.864$ Å which is the equilibrium lattice parameter for bcc Fe for the used potentials [19,20].

Before examining clusters the relaxation for a single M and a single C atom embedded in the ferrite matrix has been performed, to find the solute excess energy associated with single M and C atoms. It is assumed that M atoms only occupy substitutional bcc lattice sites of the ferrite matrix, and C atoms only occupy octahedral interstitial sites in the bcc lattice. The relaxation is performed in a supercell of $10 \times 10 \times 10$ bcc unit cells, the solute excess energies for the single embedded atoms differ less than 1 meV with the supercell with $20 \times 20 \times 20$ bcc unit cells, which is a difference smaller than 0.5 % of the solute excess energies. Therefore we conclude that the influence of the cell size is negligible. The resulting solute excess energies for the single embedded atom are taken as reference energies for a M or C atom fully dissolved, i.e., uniformly distributed, in the ferrite matrix:

$$\Delta E(X) = E(Fe_iX) - iE^c_{Fe}.\# \tag{1}$$

Where $\Delta E(X)$ is the solute excess energy ($X = M, C$), and $E(Fe_iX)$ is the total energy of the cell containing i Fe atoms and a single M or C atom. E^c_{Fe} is the cohesive energy per atom taken from [19,20], $E^c_{Fe} = -4.29$ eV, where the reference structure for Fe is bcc. For an isolated Nb atom the solute excess energy is -7.51 eV, for Ti -5.39 eV, and for C -6.06 eV (in the $10 \times 10 \times 10$ bcc unit cell supercell).

Using molecular statics, small clusters of M and C atoms are constructed within a bcc Fe crystal, these small clusters are aimed at investigating the onset formation of a M-C cluster. All clusters are, unless stated otherwise, constructed as single-layered clusters. The energy of the relaxed clusters is compared to the energy of a bcc Fe crystal where the M and C atoms are uniformly distributed in the infinitely diluted limit. To compare energies a binding energy for a supercell containing i Fe atoms, j M atoms and k C atoms with a total energy, $E(Fe_iM_jC_k)$, is determined as

$$E_{bind.} = iE^c_{Fe} + j\Delta E(M) + k\Delta E(C) - E(Fe_iM_jC_k).\# \tag{2}$$

Where $\Delta E(X)$ is defined in Eq. (1). A decrease in total energy translates to a positive binding energy, such a cluster is favourable with respect to the infinitely diluted solid solution. All clusters are simulated in various size cells, when the results differ less than 0.01 eV/atom for the atoms in the M-C cluster between sizes the interference of cell boundaries are considered negligible. This means that for several small clusters a cell containing $10 \times 10 \times 10$ bcc unit cells is used, but larger clusters were relaxed in $20 \times 20 \times 20$ or $40 \times 40 \times 20$ bcc unit cells.

To focus on the essential steps in the precipitate formation, the larger model systems contain clusters with a square shape. The square shape is the simplest shape to roughly approximate the shape observed in experiments [4,6]. The square shape greatly reduces the number of variations due to symmetry. A second advantage is that different sizes are easily determined, i.e., we may speak of a $n \times n$ square.

2.2. DFT calculations

DFT calculations were performed using projector-augmented wave (PAW) pseudo potentials as implemented in the Vienna Ab initio Simulation Package (VASP 5.3.5) [21–25].

For both M-M and M-C pairs we investigate a binding energy $E_{bind.}$ at 0 K where a positive value indicates attraction and a negative energy indicates repulsion. To evaluate the binding energy Eqs. (1) and (2) are used, where instead of the cohesive energy for Fe, E^c_{Fe}, the energy of an Fe atom in a perfect bcc lattice is calculated and used. The solute excess energies are also re-evaluated for the Nb, Ti and C atoms.

The DFT calculations are performed in supercells at a fixed volume determined by the equilibrium lattice parameter for bcc Fe which is found to be 2.833 Å. Three different supercell sizes are used all containing a perfect bcc lattice with $3 \times 3 \times 3$, $4 \times 4 \times 4$, and a $5 \times 5 \times 5$ bcc unit cells, containing 54, 128, and 250 substitutional lattice sites respectively.

For the $3 \times 3 \times 3$ supercell we use 6 k-points along all axes, the k-points are arranged following a regular Γ-centred mesh. For the $4 \times 4 \times 4$ and $5 \times 5 \times 5$ supercell we use 4 k-points along all axes, again using the regular Γ-centred mesh. The electronic wave functions are expanded in terms of plane waves up to a cut-off kinetic energy set at 400 eV for all supercell sizes. In all calculations the precision is set to medium, and convergence criteria for energy and force are set at 0.1 meV and 100 meV/nm respectively.

2.3. Molecular dynamics for Fe-Nb-C

As the formation of precipitates occurs at finite temperatures, particularly above 800 K, MD is used to simulate Fe-Nb-C clusters at finite temperatures in a supercell containing $10 \times 10 \times 10$ bcc unit cells. Simulations are performed in ferrite at 1150 K, just below the ferrite–austenite transformation temperature. Two types of system are assessed: first a system containing a random distribution of Nb and C atoms. Vacancies, zero, one or ten, are added to allow for the movement of Nb and Fe atoms. The second type is a system in which a cluster already exists, and here the stability of the cluster is tested. Again vacancies are added to allow for Nb and Fe movement.

MD simulations are performed in LAMMPS [13] using the NPT-ensemble with $P = 0$, this is done to represent realistic heating of a steel slab. Before simulation at constant temperature the supercell is heated to the chosen temperature in $1 \bullet 10^5$ time steps. The time step is set at 1 fs, and for each cell a total of $20 \bullet 10^6$ time steps are performed, so the total simulated time is 20 ns. The pressure is relaxed in 800 timesteps and the thermostat in 350 timesteps, both are chosen to avoid rapid fluctuations but still allow for equilibration well within the runtime of the simulation.

In addition to MD simulations the migration barrier for Nb and C atoms near clusters is examined using the NEB method [26] at T = 0 K. For a M atom diffusion requires the presence of a vacancy, but C atoms can move without need for vacancies, between octahedral interstitial sites. NEB calculations are performed in static crystals in $10 \times 10 \times 10$ unit cell supercells at a fixed volume where one atom is moved between an initial and final site and its neighbours are displaced following the NEB principle.

3. Results

3.1. Static relaxation

Firstly M-M pair configurations are considered, where two Nb or two Ti atoms are placed on bcc lattice sites in an Fe matrix. Binding energies of the pairs were calculated using both LAMMPS and DFT. Various pairs are illustrated in Fig. 1, the corresponding binding energies are presented in Tables 1 and 2. Secondly fifteen C-C pair configurations are considered, also presented in Fig. 1 and in Table 3. Note that positive (negative) energies mean attraction (repulsion). The comparison between the results for the MEAM potentials (in LAMMPS) and DFT reveals some important similarities with relevance for the MC carbide

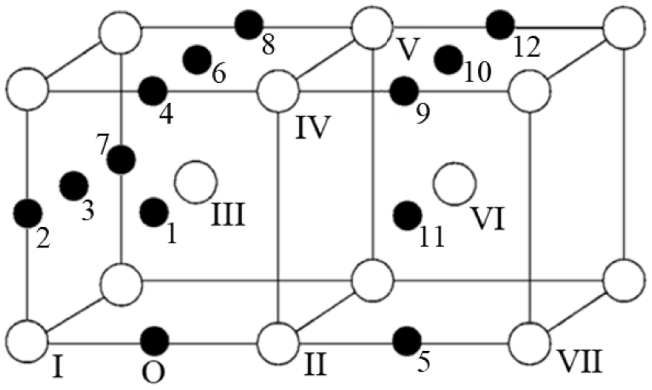

Fig. 1. Schematic representation of the M-M and M-C pairs. All M atoms are placed at the bcc lattice sites (open circles) labelled with a capital roman numeral, the carbon atoms may be placed at the closed circles labelled with Arabic numerals.

formation.

Nb and Ti carbides can form (semi-)coherent interfaces with ferrite [27,28] where the M atoms are separated roughly one ferrite lattice parameter. Hence the M-M pairs I-II, I-III, I-IV, and I-V are of great significance. The pairs with the smallest M-M separation, i.e., the I-II and I-III pairs display significant repulsive behaviour. Pairs with greater separation, the I-VI and I-VII pairs, display little interaction for the MEAM potential which even shows (small) attraction for these pairs. This indicates that the MEAM potentials will not form close M atom pairs in the absence of C atoms, in contrast to the DFT results, see Tables 1 and 2.

Interaction generally weakens when atoms are further apart, e.g., [29], but the interaction for the MEAM potentials seems especially weak. The DFT results show attraction for the I-IV Nb-Nb pair and for the I-V Ti-Ti pair, furthermore the I-VI and I-VII pairs have a repulsive interaction. For the I-II pair a repulsive interaction is found both in the LAMMPS and DFT calculations, although it is part of the coherent carbide-ferrite interface. The repulsive interaction between the M atoms at close range shows that the introduction of carbon is necessary to stabilize this pair in a larger cluster.

For the M-C pairs there is a better agreement between MEAM and DFT, albeit only as to which pairs are favoured, the actual magnitudes of the binding energy differ noticeably. For Nb-C the I-4 pair is favoured and for Ti-C the I-1 pair. There is also agreement for the C-C pairs (Table 3), where the O-3 pair is highly favoured in both MEAM and DFT.

Table 1
Pair binding energies for Nb-Nb and Nb-C pairs presented in Fig. 1. The DFT values were calculated as part of this work following Section 2.2. The LAMMPS results are from the static relaxation calculations. The most favourable (or least unfavourable) pair is marked in bold.

Nb-Nb	$E_{bind.}$ [eV] static relaxation (LAMMPS) [19]					$E_{bind.}$ [eV] DFT		
Cell size	3 × 3 × 3	4 × 4 × 4	5 × 5 × 5	10 × 10 × 10	20 × 20 × 20	3 × 3 × 3	4 × 4 × 4	5 × 5 × 5
I-II	−0.104	−0.084	−0.079	−0.074	−0.074	−0.216	−0.170	−0.148
I-III	−0.070	−0.052	−0.046	−0.041	−0.041	−0.402	−0.393	−0.335
I-IV	−0.050	−0.035	−0.030	−0.025	−0.025	**−0.016**	**−0.006**	**0.026**
I-V	−0.069	−0.046	−0.038	−0.032	−0.032	−0.053	−0.053	−0.004
I-VI	**−0.010**	**−0.005**	**0.000**	**0.004**	**0.004**	−0.040	−0.040	−0.025
I-VII	–	−0.004	−0.001	0.002	0.002	–	−0.017	0.025
Nb-C								
I-O	−1.101	−1.036	−1.021	−1.006	−1.006	−1.366	−1.209	−1.095
I-1	0.002	0.033	0.042	0.050	0.050	−0.108	−0.059	0.018
I-4	**0.207**	**0.229**	**0.237**	**0.244**	**0.244**	**−0.103**	**0.070**	**0.102**
I-5	−0.090	−0.065	−0.055	−0.050	−0.049	−0.318	−0.213	−0.145
I-6	−0.045	−0.032	−0.027	−0.022	−0.022	−0.271	−0.097	−0.047
I-8	−0.025	0.005	0.016	0.024	0.024	−0.142	0.018	0.068
I-9	−0.031	−0.030	−0.021	−0.017	−0.015	−0.078	0.012	0.063
I-10	−0.027	−0.015	−0.005	0.002	0.003	−0.089	0.016	0.064
I-11	−0.003	0.011	0.020	0.028	0.028	−0.062	0.023	0.062
I-12	−0.057	−0.058	−0.047	−0.040	−0.039	−0.119	−0.046	0.014

Table 2
Pair binding energies for Ti-Ti and Ti-C pairs presented in Fig. 1. The DFT values were calculated as part of this work following Section 2.2. The LAMMPS results are from the static relaxation calculations. The most favourable (or least unfavourable) pair is marked in bold.

Ti-Ti	$E_{bind.}$ [eV] static relaxation (LAMMPS) [20]					$E_{bind.}$ [eV] DFT		
Cell size	3 × 3 × 3	4 × 4 × 4	5 × 5 × 5	10 × 10 × 10	20 × 20 × 20	3 × 3 × 3	4 × 4 × 4	5 × 5 × 5
I-II	−0.047	−0.024	−0.024	−0.024	−0.024	−0.143	−0.136	−0.160
I-III	−0.293	−0.278	−0.277	−0.275	−0.275	−0.237	−0.249	−0.249
I-IV	−0.012	−0.021	−0.019	−0.019	−0.019	0.007	−0.009	−0.016
I-V	−0.026	−0.030	−0.027	−0.026	−0.026	**0.019**	**0.011**	**0.010**
I-VI	**0.017**	**0.012**	**0.014**	**0.014**	**0.014**	−0.047	−0.024	−0.027
I-VII	–	−0.019	−0.017	−0.017	−0.017	–	−0.017	−0.013
Ti-C								
I-O	−0.851	−0.818	−0.805	−0.791	−0.790	−0.817	−0.728	−0.628
I-1	**0.172**	**0.186**	**0.189**	**0.192**	**0.192**	**0.012**	0.038	0.093
I-4	0.145	0.141	0.144	0.146	0.145	−0.022	**0.103**	**0.128**
I-5	−0.026	0.006	0.005	0.008	0.009	−0.158	−0.103	−0.069
I-6	−0.042	−0.052	−0.053	−0.052	−0.052	−0.150	−0.027	0.005
I-8	−0.036	−0.018	−0.012	−0.009	−0.009	−0.090	0.033	0.057
I-9	−0.017	−0.019	−0.017	−0.015	−0.015	−0.023	0.040	0.063
I-10	−0.004	0.005	0.007	0.010	0.009	−0.039	0.033	0.061
I-11	−0.019	−0.013	−0.008	−0.005	−0.005	−0.040	0.041	0.051
I-12	−0.033	−0.038	−0.038	−0.036	−0.036	−0.059	−0.012	0.024

Table 3
C-C pair binding energies for various C-C pairs illustrated in Fig. 1, demonstrating the supercell size effect. The DFT values were calculated as part of this work following Section 2.2. The LAMMPS results are from the static relaxation calculations. In each column the most favourable (or least unfavourable) pair is marked in bold.

C-C	$E_{bind.}$ [eV] static relaxation (LAMMPS) [19,20]					$E_{bind.}$ [eV] DFT		
Cell size	3 × 3 × 3	4 × 4 × 4	5 × 5 × 5	10 × 10 × 10	20 × 20 × 20	3 × 3 × 3	4 × 4 × 4	5 × 5 × 5
O-1[†]	–	–	–	–	<−3.000	−2.027	−1.916	−1.863
O-2	−1.256	−1.209	−1.198	−1.189	−1.188	−0.861	−0.775	−0.700
O-3	−0.051	0.016	0.040	0.060	0.062	−0.331	−0.221	−0.118
O-4	0.228	0.294	0.314	0.334	0.335	−0.098	0.030	0.136
O-5	−4.940	−2.296	−1.972	−1.899	−1.892	−3.434	−1.923	−1.655
O-6	**0.362**	**0.347**	**0.348**	**0.352**	**0.352**	−0.067	0.005	0.083
O-7	0.168	0.185	0.193	0.201	0.201	−0.112	−0.024	0.058
O-8	−0.374	−0.245	−0.202	−0.170	−0.168	−0.147	−0.006	0.092
O-9	−0.029	0.015	0.037	0.059	0.060	−0.229	−0.118	−0.004
O-10	−0.066	0.000	0.008	0.011	0.010	−0.266	−0.115	−0.029
2-11	−0.069	−0.042	−0.032	−0.021	−0.021	−0.191	−0.026	0.032
2-9	−0.079	−0.035	−0.032	−0.034	−0.034	−0.192	−0.019	0.061
2-10	−0.003	0.030	0.056	0.083	0.084	−0.095	**0.035**	**0.142**
3-12	−0.284	−0.199	−0.156	−0.128	−0.127	−0.395	−0.251	−0.131
O-12	−0.051	−0.011	0.016	0.040	0.042	**−0.057**	−0.006	0.103

[†] The O-1 pair always relaxes to a 2-11 pair using the MEAM potential.

Moreover, the C-C pairs display significantly positive binding energies. Therefore C clusters may easily form, and are expected to act as a catalyst for the formation of M-C clusters, as shown in Fig. 2.

From the analysis of the various pair interactions of M and C atoms a pattern seems to exist. Both Nb and Ti prefer similar M-C pair configurations. For the M-M pairs there is a slight difference, where the Nb-Nb pair prefers a I-IV pair (for MEAM only for both M atoms within the same bcc unit cell) and Ti-Ti prefers I-V (also within the same unit cell). The energy difference between the I-IV and I-V pair is small. So there seem to be some parallels between both metals, particularly when we consider the DFT results. Both metals have similar metal bond lengths [30], a key difference however is that the Ti atoms are smaller when embedded in the bcc Fe matrix [31]. This lowers matrix strain around the Ti atoms compared to the strain caused by the Nb atoms.

From simple pairs larger clusters are constructed by adding atoms in various positions on the bcc lattice for M atoms (i.e., replacing an Fe atom) and its octahedral interstitial positions for C atoms. These clusters are made to simulate the onset of M-C cluster formation. It is found that C clusters have highly favourable binding energies, adding C atoms to a pre-existing C cluster can increase the binding energy more than the

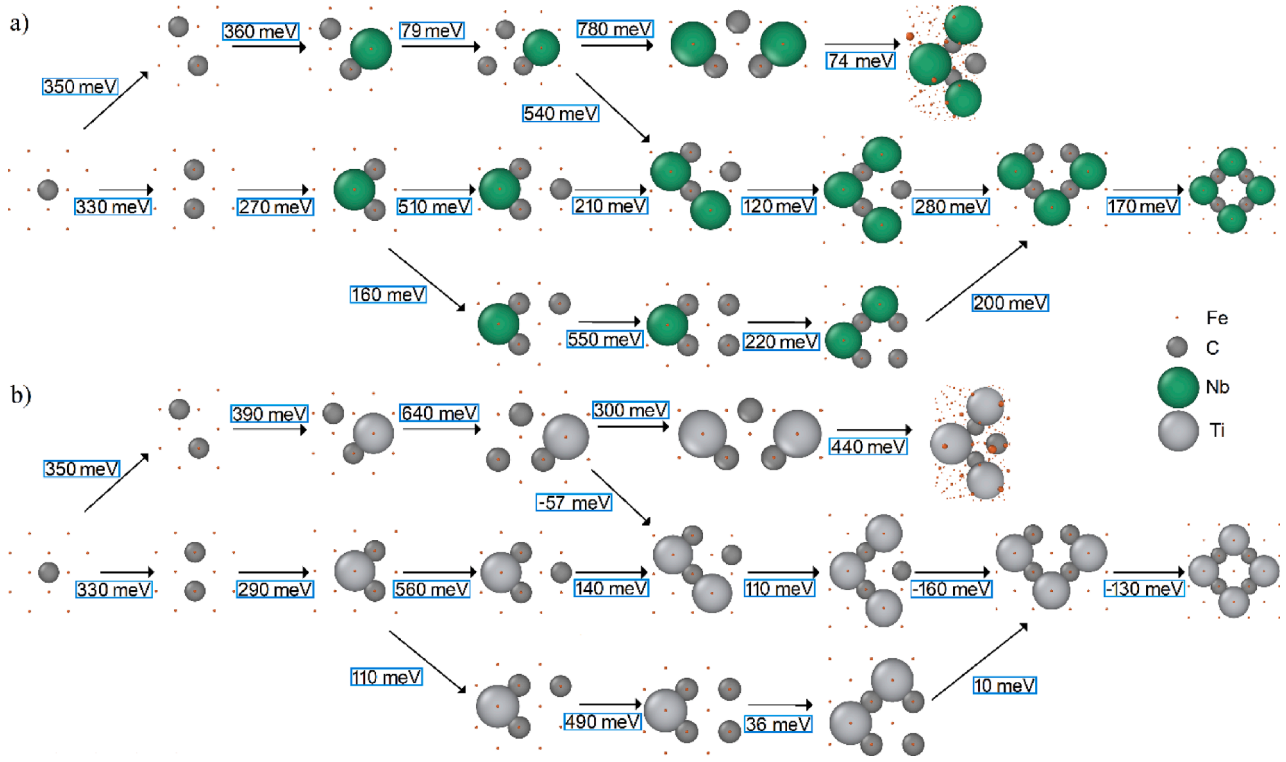

Fig. 2. Growth path of a M-C cluster in a bcc Fe matrix, calculated with a MEAM potential [19,20] for static relaxations in LAMMPS. The clusters displayed here all lie within the same (1 0 0) plane can therefore be viewed as 2D clusters (except for the rightmost cluster in the top row, where the C atoms do not lie in the same (1 0 0) plane as the Ti atoms). For each added atom the gain in binding energy from the previous cluster is given displaying that there is a path along which each added atom gains additional binding energy for the cluster. Shown clusters are unrelaxed for clarity, however corresponding binding energies are presented for the relaxed clusters. Fe atoms are scaled down for clarity. In a) Nb-C clusters are shown and in b) Ti-C clusters. NB in MD simulations we observe that the C atoms (for small $FeMC_3$ clusters) relax slightly out of the (1 0 0) plane containing the M atoms, see Fig. 4c.

binding of the most favourable C-C pair. Combined with the high mobility of C atoms in the ferrite matrix it is concluded that C clusters will form quickly. From the C-C pair interactions we find that the C atom clustering is an ordering effect, as for the various C atoms in the random solution a lot of energy can be gained by forming pairs and larger clusters. We note that for higher C concentrations at temperatures below 800 K spinodal decomposition of the Fe-C solid solution is observed, e.g., [32–39].

In Fig. 2 several evolution paths, starting from a single C atom, are presented for a M-C cluster inhabiting a single (1 0 0) plane. For each atom addition the gain in binding energy is shown. We selectively display paths with favourable binding energy gain for each added atom using Eq. (2). These small clusters remain coherent with the bcc lattice after relaxation, and show a (Fe,M)C-like character.

We remark that the (Fe,M)C clusters found in Fig. 2 display a distinct pattern where the Fe and M atoms lie in a 'checkerboard pattern'. The emergence of this pattern is likely tied to the matrix strain caused by the size differences between M and Fe atoms as the [1 0 0] direction is the elastically soft direction in bcc Fe. Such a checkerboard pattern allows for the observed coherency between the (Fe,M)C cluster lying in a (1 0 0) plane and its adjacent (1 0 0) planes in the matrix. In Fig. 3 the ring-shaped cluster shown in Fig. 2 is expanded, in Table 4 the binding energies for added atoms are given. The C atoms also form a particular pattern, which is fully described in Section 3.2. Using this pattern the most favourable growth is found to be in-plane. There are sites out of the (1 0 0) habit plane of the cluster onto which M atoms can attach, but these are not the most favourable sites. The C atoms enhance the in-plane growth of the checkerboard pattern as shown in Table 4.

We label the (Fe,M)C clusters as proto-precipitates, which we consider to be the earliest stages of nano-precipitate formation. Direct construction of a 2D NaCl-structured cluster is not favoured. For both Ti-C and Nb-C clusters a similar behaviour is observed where clusters are formed that lie in the {1 0 0} planes of the ferrite matrix, which is also found for nano-precipitates observed in experiments [3–9]. Note that the relaxations are performed at 0 K, so thermal effects are not present.

Table 4
Change in binding energy for atoms added in Fig. 3 under static relaxation. The C atoms want to attach in the adjacent (1 0 0) planes in a pattern shown in Fig. 3. M atoms continue the checkerboard pattern found in Fig. 2.

C and Nb atoms [19]

Added atom	$\Delta E_{bind.}$ [eV]	Added atom	$\Delta E_{bind.}$ [eV]	Added atom	$\Delta E_{bind.}$ [eV]
a	0.602	a, A	0.510	a, b, c, A	1.939
b	0.190	a, B	0.512	a, b, c, B	1.887
c	−0.294	a, C	0.576	a, b, c, C	2.073
a, b	1.366	a, D	0.793	a, b, c, D	2.257
a, c	0.903	a, E	0.805	a, b, c, E	2.020
b, c	0.434	a, F	−0.349	a, b, c, F	1.197
a, b, c	2.005	a, G	0.642	a, b, c, G	2.006

C and Ti atoms [20]

Added atom	$\Delta E_{bind.}$ [eV]	Added atom	$\Delta E_{bind.}$ [eV]	Added atom	$\Delta E_{bind.}$ [eV]
a	1.261	a, A	1.222	a, b, c, A	2.879
b	1.116	a, B	1.108	a, b, c, B	2.841
c	0.495	a, C	1.250	a, b, c, C	2.996
a, b	2.195	a, D	1.330	a, b, c, D	3.170
a, c	1.585	a, E	1.340	a, b, c, E	2.856
b, c	1.398	a, F	0.687	a, b, c, F	2.342
a, b, c	2.924	a, G	1.527	a, b, c, G	3.167

In Fig. 2 it is shown that clusters tend to start from a C cluster (here a C-C pair). The two C-C pairs shown in Fig. 2 have a higher binding energy than the shown M-C pairs in Table 3. Moreover, bonding of a M atom to each C-C pair increases the total binding energy more than the binding of a single M atom to a C atom. This result shows that C-C pairs (and clusters), which can form through Fe-C spinodal decomposition, or as a temporal fluctuation, are essential for the formation of M-C clusters, as the M atoms do not display attractive interaction for the M-M pairs in

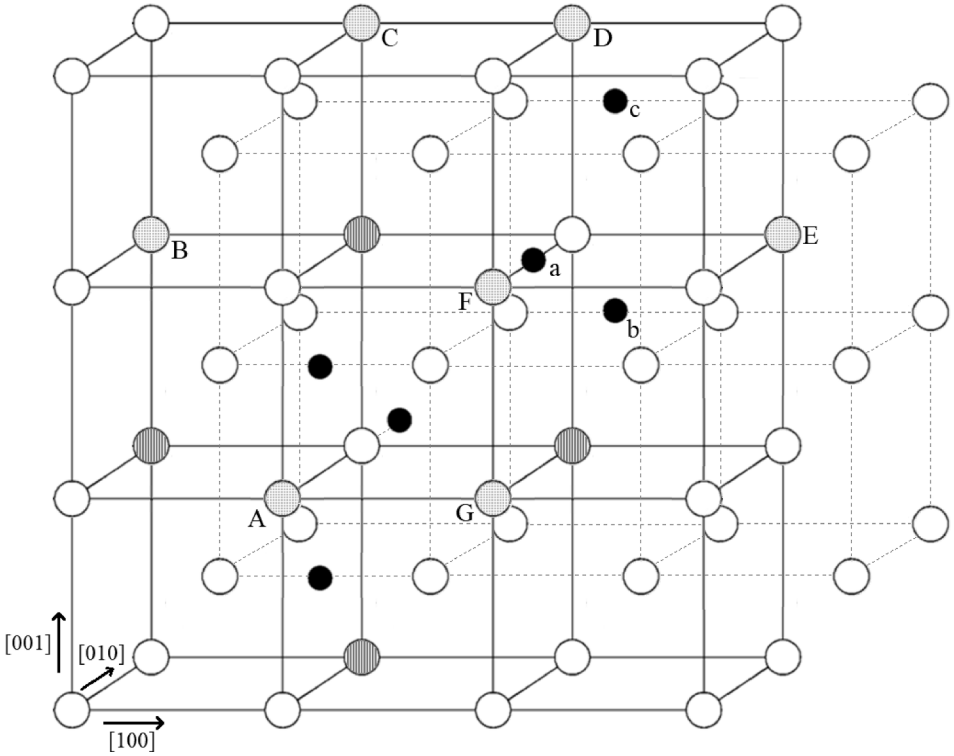

Fig. 3. The continuation of the growth of clusters shown in Fig. 2, again the clusters are unrelaxed for clarity. The initial M atoms are given by the striped dark grey bcc sites. The initial C atoms are out-of-M-plane and depicted by the black circles, this displaced form is more stable than what is depicted in Fig. 2. New M atoms are added at the light grey bcc sites marked by upper case letters, C atoms are added at the black sites labelled with lower case letters.

Tables 1 and 2. Moreover, as some M-M pairs are favourable according to the DFT data, it is worthwhile to note that the bond between M and C atoms is more favourable.

The next step is to investigate the role of vacancies. It is observed, in simulations, that the zone around the cluster, the 'transition envelope' or 'transition zone', attracts vacancies. The existence of vacancies in this envelope reduces the strain near the cluster, which was also noticed for TiC [6,40]. The clusters also attract vacancies inside the cluster's (1 0 0) habit plane, particularly at the sites where the Fe atoms are in the checkerboard pattern. The vacancies lower the local strain, as the M atoms are generally large compared to the Fe atoms. Moreover the MEAM potential has a strong positive vacancy C atom bond [41].

NEB is used to determine migration barriers for Nb and C atoms near various clusters and at various sites. In some cases the migration barrier for C atoms is decreased near C atoms, particularly in the same (1 0 0) plane. This effect is caused by the straining of the ferrite matrix by the C interstitials. The migration barrier for a single C atom in ferrite is 0.77 eV from one octahedral site to a neighbouring octahedral site, e.g., from site 2 to 3 in Fig. 1. However moving a C atom from a C-C pair oriented as O-2 in Fig. 1 to form O-3 has a barrier of 0.58 eV a reduction of almost 25 %. For larger C clusters, e.g., for C atoms at O-2-4 (Fig. 1) the barrier for the C atom from site 4 moving away from the site 2 atom along the line defined by their initial positions is 0.42 eV, which is a reduction of 45 %. In general the presence of a C cluster lowers the migration barriers for C atoms within strained planes.

For Nb atoms the opposite is true, as the Nb atoms are significantly larger than Fe atoms the presence of C atoms increases the migration barrier. Using NEB simulation in LAMMPS the migration of a Nb atom to a nearest neighbour (1NN) vacancy is 0.35 eV, which is comparable to the migration barrier for Fe atoms to a 1NN vacancy which is 0.47 eV (for DFT data cf. [42]). Note that the vacancy formation energy next to a Nb atom is 0.05 eV lower than in the Fe matrix, i.e., the vacancy is bonded with 0.05 eV (DFT returns 0.35 eV [42]). The migration barrier for a Nb atom at site III near a C-C pair at sites O and 2 (Fig. 1) to site I is almost tripled at 1.03 eV. Similar increases are observed near larger Nb-C clusters, particularly for the movement of Nb atoms not in the (1 0 0) plane of the cluster. It is therefore concluded that Nb atoms do not easily move through C clusters, but rather that they remain on the surface of existing C clusters. This does not mean that the Nb layer remains on top of a C cluster as C atoms can attach from bulk and embed the Nb-rich layer, alternatively C atoms from the cluster can move to embed the Nb atoms.

An exception exists for Nb atoms near a cluster, in the same (1 0 0) plane as the cluster. These Nb atoms can have a lowered migration barrier for movement in the [1 0 0] direction of the cluster, we found barriers as low as 0.21 eV. Where Nb atoms attach to the edge of a (Fe, Nb)C cluster as this is favourable for the binding energy. Which further validates the in-plane growth of (Fe,Nb)C clusters as described above.

The same effects are witnessed for Ti atoms, but as the Ti atoms are smaller than the Nb atoms in the bcc Fe matrix [31] the effects are weaker.

3.2. Molecular dynamics

MD simulations at non-zero temperatures are performed for the Fe-Nb-C ternary system. As the Ti and Nb results are very similar only the results for Nb are presented.

Cluster formation in Fe-Nb-C is simulated in a supercell of $10 \times 10 \times 10$ bcc unit cells. To increase the rate at which clusters can form [43,44], simulations are performed at somewhat elevated Nb and C concentrations of roughly 0.5 %at. and 1 %at. The formation of C clusters occurs within a few ns at 1150 K. However only one or two Nb atoms attach to the formed C cluster within the run-time of the simulation, displaying minimal Nb-C cluster formation for various Nb, C, and vacancy concentrations. Note that a vacancy concentration of one vacancy in the $10 \times 10 \times 10$ bcc unit supercell exceeds the equilibrium concentration by a factor of 13600, so even at these vacancy concentrations the simulation time is too short to see cluster formation. The simulated time is 20 ns, but at such vacancy concentrations the number of possible vacancy jumps is much higher than would be possible at the expected vacancy concentration. Therefore a corrected simulated time can be estimated at $13600 \bullet 20$ ns for the cell with 1 vacancy. Here it is noted that the increase in possible jumps mainly occurs for Fe and Nb atoms as they are dependent on vacancies for diffusion, much less so for C atoms which move between octahedral interstitial sites without relying on vacancies in the bcc lattice. This needs to be taken into account if one wishes to adjust the simulated time.

It may be concluded that the formation of Nb-C clusters takes much more than 20 ns even at 1150 K (cf. Hin et al. [43,44]) making it unpractical for our purposes. The formation of C clusters has been examined experimentally [32–35], the formation of C clusters happens spontaneously as a local ordering effect, where the M atoms can act as anchors for the C atom clusters. These experimental results for C atom clustering are reflected by the MD simulations. The experimentally observed C clusters form in parallel {1 0 0} layers [34], while Nb atoms migrate to the surface of C clusters, which provides the basic steps in the formation of a proto-precipitate.

As the focus of this work is on the formation of M-C clusters, which take too long to form in MD simulations, a cluster is constructed, as shown in Fig. 4a. This constructed cluster is used to assess the stability of the (Fe,M)C cluster, and to study the movement of C atoms around the cluster. The MD simulations are performed at 1150 K. The system is simulated with varying numbers of vacancies, namely 0, 1, and 10. Note that even at 1150 K the expected fraction of vacancies is $e^{-E^f_{vac}/kT} = 3.67 \times 10^{-8}$, where E^f_{vac} is the vacancy formation energy in the ferrite matrix which is 1.7 eV for the used potential [19,20].

In these simulations it is found that the C atoms in an initial cluster as depicted in Fig. 4a move to form a cluster as presented (idealised) in Fig. 4b and detailed further in Fig. 4c and 4d, here the Nb atoms barely move with one vacancy, and still remain somewhat clustered when there are 10 vacancies. This could be a result from vacancies binding to the cluster atoms. In Fig. 4b, 4c, 4d and 4e the Nb-C cluster extends into its adjacent (1 0 0) planes as C atoms are placed on top of the (1 0 0) plane containing Nb, as we already found in Fig. 3 and Table 4. In fact the C atoms form 'triangles' around the Fe atoms in the cluster, as shown in Fig. 4b, 4c, and 4d (also cf. [45]). We note specific features for the M-C cluster:

- The Fe and M atoms form a checkerboard-pattern as shown in Fig. 4.
- We can distinguish two types of C atoms; i) C lying in 'rows' with two C atoms (near a Fe site) on one side of the cluster, and ii) C atoms lying 'between-rows'. The rows, ideally, lie alternating on both sides of the Fe-M checkerboard pattern situated in a single (1 0 0) plane. This is displayed in Fig. 4c and 4d.
- Fe atoms in the cluster have three close C neighbours. Two within a 'row', the other C atom lies 'between-rows'. The Fe-C distance is roughly equal for all three C atoms, hence the C atoms form a triangle around the Fe atom. The Fe-C bonds are shown in Fig. 4c.
- Moreover, the (Fe,M)C cluster found here has a composition of $FeMC_3$ where the M atoms are outnumbered 1:3 by C atoms. NB, the platelet might contain even more C atoms because the M atoms attach to (larger) C clusters so that the platelet surface is enriched in C.

In the MD simulations (Fe,Nb)C clusters are observed that are coherent with the bcc lattice. The structure of the cluster however differs from the NaCl-structure as described above. The (Fe,M)C cluster has a high Fe and C concentration, these high concentrations are explained by the earlier observation that M atoms are attracted by C clusters. Moreover, the structure of the (Fe,M)C cluster displays an ordering deviating from the NaCl structure, whereas the NaCl-structure is most stable for

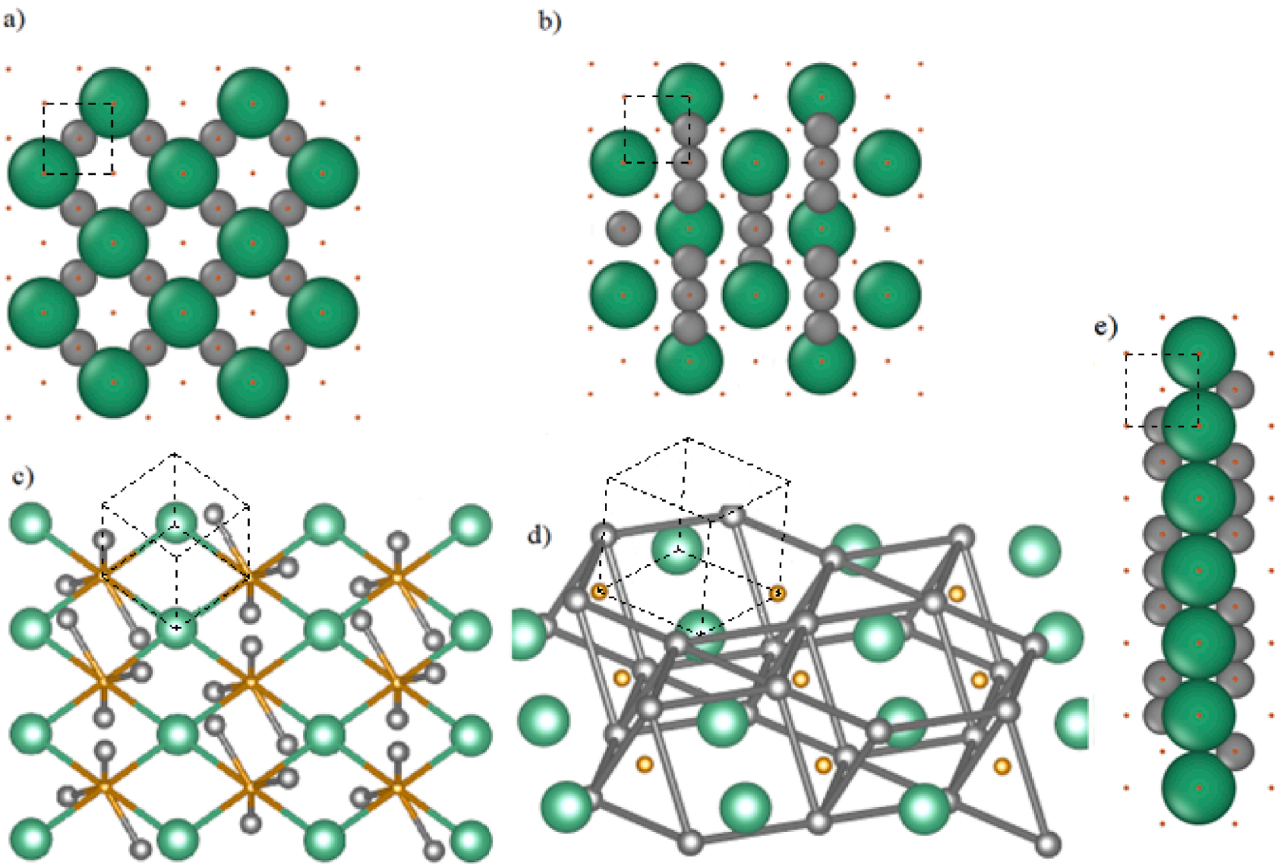

Fig. 4. a) The initial cluster used in MD simulations. Different colours are used for the various atoms the C atoms are grey, the M atoms are green (largest), and the Fe atoms are brown (smallest). b), c), d) and e) are strongly idealized (and unrelaxed for clarity) version of the most stable cluster as found from MD simulations. In b) a front-view of the cluster is shown, c) the (1 0 0) plane in which the Fe and Nb atoms are indicated by the Fe-Nb bonds as well as the C atoms that lie in the adjacent (1 0 0) plane indicated by the Fe-C bonds. In d) the C-C bonds shorter than 3.5 Å are depicted, from which the C 'triangles' around the Fe atoms are shown. (also cf. supplemental data [45]). Note that the edges of the cluster displayed in Figures b),c), and d) are likely to be 'decorated' with more C atoms, an example is given in Fig. 5b–5d. In e) the side of a cluster is shown to demonstrate how the C atoms lie out of the habit plane of the cluster. In each figure the bcc unit cell is outlined by the black dashed lines.

pure NbC [46], and is observed for larger precipitates [12]. The transformation of the (Fe,M)C cluster to a NaCl structured cluster is studied in [18].

3.3. Stability of clusters at finite temperatures

In Section 3.1 the initial stage of Fe-M-C clustering has been shown, and in Section 3.2 the behaviour of a larger (Fe,M)C cluster at finite temperatures has been investigated where an ordered $FeMC_3$ cluster is identified as a very stable configuration.

Relaxing clusters at 0 K shows various clusters that have a favourable binding energy, however the stability at finite temperatures remains unknown. To factor in thermal effects an estimate for the change in entropy is made. For the entropy term the configurational term is taken as it is the most dominant contribution and approximated as ideal mixing. Other, e.g., vibrational contributions are collected in a polynomial in the composition as in [47], as the matrix fractions for M and C atoms are small a first-order approximation suffices. Then the other entropy contributions are reduced to a constant excess embedding energy, G_{xs}^{emb}, which is dominated by the ideal mixing entropy, so for simplicity only the configurational entropy is considered. Then the entropy of the matrix is given as

$$S = k \bullet \ln(\omega), \# \tag{3}$$

where ω is the number of configurations, and k the Boltzmann constant. We define N_{Fe}, N_M, N_{vac}, N_C, N_{vacoct}, as the number of Fe, M, vacancies, C, and vacant octahedral interstitial sites respectively. The total number of lattice sites can be defined as $\overline{N}$ where $\overline{N} = N_{Fe} + N_M + N_{vac}$, then $N_C + N_{vacoct} = 3\overline{N}$. Here it is implicitly assumed that Fe and Nb atoms can only occupy bcc lattice sites, and C atoms can only occupy octahedral interstitial sites. Then for an ideal mixture:

$$\omega = \frac{\overline{N}!}{N_{Fe}!N_M!N_{vac}!} \bullet \frac{(3\overline{N})!}{N_C!N_{vacoct}!}.\# \tag{4}$$

Now defining the fractions $X_i = N_i/\overline{N}$ for $i = \{Fe, M, vac\}$, and $Y_j = N_j/(3\overline{N})$ for $j = \{C, vacoct\}$ and using Stirling's approximation it is found that for a system of size $\overline{N}$

$$\ln(\omega) = -\overline{N}\left(\sum_i X_i \ln(X_i) + 3 \bullet \sum_j Y_j \ln(Y_j)\right).\# \tag{5}$$

For the estimation of the stability of a cluster we compare a system in which all clusters are dissolved, of which $\ln(\omega)$ is given by Equation (5), and a system with one cluster consisting of $N_{Fe}^{cl}, N_M^{cl}, N_C^{cl}$, and N_{vac}^{cl} sites, the number of Fe, Nb, C, and vacancies in the cluster respectively. Assuming that $\overline{N^{cl}} = N_{Fe}^{cl} + N_M^{cl} + N_{vac}^{cl}$ and N_C^{cl} are small the change in entropy in the matrix is

$$\Delta S^{matrix} = k \bullet \Delta\ln(\omega) = k \bullet \overline{N^{cl}}\left(\sum_i X_i \ln(X_i) + 3 \bullet \sum_j Y_j \ln(Y_j)\right).\# \tag{6}$$

Because the cluster is an ordered structure its configurational

entropy is assumed to be negligible compared to the entropy change in the matrix. As X_M, Y_C, and X_{vac} are small, the entropy per alloy atom can be written as

$$S_M = -k \bullet \ln(X_M), S_C = -k \bullet \ln(Y_C), \text{and} S_{vac} = -k \bullet \ln(X_{vac}).\# \quad (7)$$

Then for every atom that goes from solid solution to a cluster, the corresponding amount of entropy is lost.

The entropy contribution at a given temperature T can be compared directly to the binding energies found in the static relaxation. This is possible as the concentrations of M and C atoms in micro-alloyed steels are generally quite low ($0.05\%_{at.}$ for M and $0.15\%_{at.}$ for C). As the concentrations are so low, M and C atoms can be randomly placed in the ferrite matrix (still assuming M atoms only occupy substitutional sites of the bcc lattice, and C atoms occupy octahedral interstitial sites) without interaction. So the energies associated with fully dissolved atoms are good estimates for the mixing enthalpy ΔH_{mix}. The change in free energy due to the forming of a cluster can be written as

$$\Delta G = G^{matrix} - G^{clus} = \left(H^{matrix} - TS^{matrix}\right) - \left(H^{clus} - TS^{clus}\right) = \left(H^{matrix} - H^{clus}\right) - T\Delta S^{matrix} \approx E_{bind} - T\Delta S^{matrix}.\# \quad (8)$$

When comparing the binding energy of a cluster to the change in entropy of mixing it is possible to show whether or not it is energetically favourable to form the cluster with respect to the solid solution at the bulk composition at finite temperatures. Note that the existence of more stable clusters with the same number of atoms cannot be excluded.

Applying the Gibbs energy assessment to various clusters shows that there are several M-C clusters that are energetically favourable well into the $>$ 1000 K range where MC precipitation is also observed. The stabilising factor lies with the C cluster, which plays a key role in stabilising proto-precipitates. For several clusters T_0, the 'T$_0$-temperature' where two phases of identical chemical composition have the same Gibbs energy, i.e., the temperature at which $T_0 \Delta S = E_{bind.}$ is presented in Fig. 5a. In Fig. 5a we simulate clusters that use the same 'triangular' pattern as presented in Fig. 4b, 4c and 4d, but now the edges are decorated with C atoms as shown in Fig. 5b–5d (cf. [45]). 'Decorated' means that the edges of the clusters, i.e., in the habit plane, are also covered with C atoms.

In Fig. 5a the M fraction is kept constant at $X_M = 0.0005$ for all supercells, the carbon fraction is fixed at $X_C = 0.0015$. It is noted that the T$_0$-temperature for small clusters is lower than for larger clusters, indicating that clusters become more stable with increasing cluster size as the T$_0$-temperature increases with cluster size.

Fig. 5a shows that the $FeMC_3$ clusters are stable up to approximately 1100 K for $FeNbC_3$, and 1175 K for $FeTiC_3$. These temperatures are well in the experimental temperature range for which the platelets were observed [3–9]. Note that the ferrite matrix undergoes a phase transformation to austenite (fcc) at 1185 K, so larger Ti-C clusters are nearly always stable in ferrite at typical C and Ti concentrations, i.e., $X_{Ti} \approx 0.0005$ and $X_C \approx 0.0015$.

4. Formation mechanism

From simulations both static and dynamic, and the thermodynamic assessment the following hypothesis for a formation path is derived:

- Initially C atoms form clusters in the {1 0 0} planes of the ferrite matrix through spinodal decomposition, or as a temporal fluctuation. The bcc Fe lattice is strained around these C clusters. Migration of C atoms in the (1 0 0) plane of a cluster is increased as migration barriers are lowered.
- In the strained zone around the C cluster M atoms attach to the surface of C clusters, as there is an attraction between the C cluster and M atoms. M atoms hardly move out of the cluster once attached to a (Fe,M)C cluster due to high migration barriers around the cluster. C atoms can attach to the cluster with favourable effect on the binding energy, thus the Nb-rich layer can be embedded in a C cluster. Both processes occur simultaneously where growth of the cluster is favoured in a single (1 0 0) plane.

In this process of M atoms attaching to the cluster a $FeMC_3$ cluster is formed. Clusters can form containing as little as two or three M atoms. Such proto-precipitates have a diameter less than 1 nm.

The formation of $FeMC_3$ clusters presents a precursor stage to the formation of NaCl-structured platelets. The mechanism found in this work presents an atomistic picture describing the processes that lead to the formation of the nano-precipitates (platelets) found in experiments [3–9]. However the carbon content of the clusters, found in the simulations, is outnumbering M atoms 3:1. Some factors may contribute to this high carbon content.

We note that C atoms may form clusters through temporal

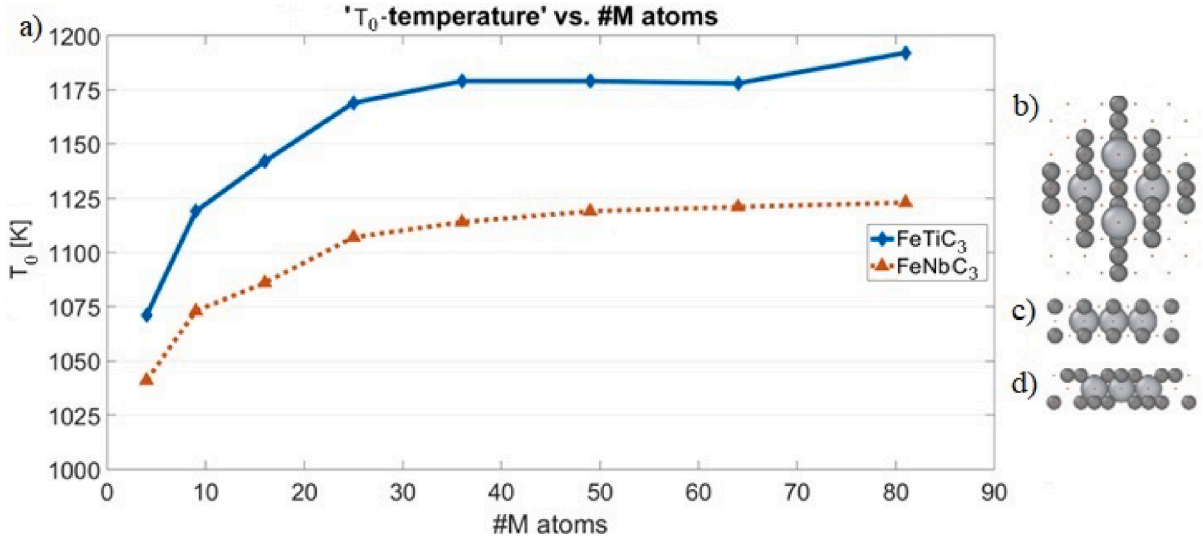

Fig. 5. a) T$_0$-temperature for TiC and NbC clusters calculated using the entropy of mixing from Eq. (6). The solid blue line belongs to the (Fe,Ti)C cluster, and the red dotted line belongs to the (Fe,Nb)C cluster. The fraction $X_M = 0.0005$ is fixed, and the C fraction is fixed at $X_C = 0.0015$. The Ti cluster remains energetically favourable up to higher temperatures than the Nb cluster, this is in agreement with the solubility products of the NbC and TiC carbides [48]. In b) the top-view of an (Fe,M)C cluster is given with added excess C atoms, in c) and d) two sides of the (Fe,M)C cluster are presented. The patterns given in b)–d) are extended for the larger clusters.

fluctuations in ferrite, but the formation of C-rich zones may also occur in austenite [49–51]. The formation of a M-C cluster pins part of the C atoms in a carbide precipitate. Contrary to [8] we find that the formation of C fluctuations occurs first and possibly preferentially near M atoms. We observe that the M atoms are attracted to C clusters to form proto-precipitates. Some C-rich layers found in spinodal decomposition [36] could attract M atoms and be stabilised to form $FeMC_3$ clusters. We find that carbides form at sites where C atoms accumulate and form clusters, despite the fact that M atoms are generally less mobile than C atoms. This effect, where the C atoms determine the position of the precipitate rather than the M atoms, was previously observed in Monte-Carlo simulations [43,44]. Following the cluster formation path found in this work, this counterintuitive result is explained by the fact that M atoms are inclined to attach to C clusters, rather than form independent M clusters.

We have shown that the formation of M-C clusters encompasses several steps. Firstly the fluctuation of C atoms in ferrite forms rapidly evolving C clusters in the {1 0 0} planes of the ferrite matrix [32–36]. Secondly M atoms attach to the C clusters, as is shown by the favourable binding energies. The M atoms thereby play a stabilising role on the C fluctuations by forming a M-C cluster. Alternately, the C clusters and fluctuations are more likely to occur near M atoms. Moreover, clusters attract vacancies [18], and the Nb (or Ti) migration energy is lowered in a (1 0 0) plane in which a cluster is situated.

The M-C clusters lie in the {1 0 0} planes of the ferrite matrix like the C clusters, and they form in a single (1 0 0) plane. The initial M-C clusters contain a large fraction of Fe and C atoms with a $FeMC_3$ stoichiometry. The $FeMC_3$ cluster has a structure where the C atoms do not lie in the NaCl-structure sites, but they rather form a structure where 2/3 of the C atoms align in 'rows' alternating between either surface of the cluster and the adjacent Fe lattice planes. The remaining C atoms lie directly between these 'rows'.

5. Conclusions

Formation of M-carbides in ferrite encompasses different stages. Before the actual formation of a M-C cluster C atoms form clusters in the {1 0 0} planes of the ferrite matrix as a result of fluctuations. Unto these C clusters M atoms attach to form ordered Fe-M-C clusters with a composition $FeMC_{3+x}$, also directed in the [1 0 0] directions of the ferrite matrix. The M atoms in a $FeMC_{3+x}$ cluster lie within a single (1 0 0) plane, where they form a checkerboard pattern together with Fe atoms. The origins of this checkerboard pattern seem to lie in the pair interactions between the M atoms which is particularly pronounced in DFT calculations.

Growth simulations reveal a stable $FeMC_3$ proto-precipitate and MD simulations show that at elevated temperatures it remains coherent with the ferrite matrix. At common matrix fractions, $X_{Nb(orTi)} \approx 0.0005$ and $X_C \approx 0.0015$, the $FeNbC_3$ clusters are stable in the 1100 K range, and the $FeTiC_3$ clusters remain stable near 1185 K which is the ferrite–austenite transition temperature.

Hence the $FeMC_3$ proto-precipitates found in this study represent a very plausible precursor to MC nano-precipitate carbides.

Funding

This research was carried out under project number T17019m in the framework of the Research Program of the Materials Innovation Institute (M2i) supported by the Dutch government.

CRediT authorship contribution statement

R.J. Slooter: Writing – original draft, Visualization, Writing – review & editing, Data curation, Investigation, Formal analysis, Software, Methodology, Conceptualization. **M.H.F. Sluiter:** Supervision, Funding acquisition, Project administration, Writing – review & editing, Data curation, Resources, Investigation, Formal analysis, Validation, Software, Methodology, Conceptualization. **W.G.T. Kranendonk:** Supervision, Writing – review & editing, Resources, Investigation, Formal analysis, Validation, Conceptualization. **C. Bos:** Supervision, Writing – review & editing, Formal analysis, Validation, Conceptualization.

Declaration of Competing Interest

The authors declare that they have no known competing financial interests or personal relationships that could have appeared to influence the work reported in this paper.

Data availability

All research data can be obtained by requesting the corresponding author. The used MEAM potentials are readily available at OpenKIM.org.

Appendix A. Supplementary material

Supplementary data to this article can be found online at https://doi.org/10.1016/j.commatsci.2023.112455.

References

[1] P.A. Manohar, M. Ferry, T. Chandra, ISIJ Int. 38 (1988) 913–924.
[2] E. Nes, N. Ryum, O. Hunderi, Acta Metall. 33 (1985) 11–22.
[3] E. Courtois, T. Epicier, C. Scott, Mater. Sci. Forum 500–501 (2005) 669–676.
[4] A.J. Breen, K.Y. Xie, M.P. Moody, B. Gault, H.-W. Yen, C.C. Wong, J.M. Cairney, S. P. Ringer, Microsc. Micranal. 20 (2014) 1100–1110.
[5] J. Takahashi, K. Kawakami, Y. Kobayashi, Acta Mater. 153 (2018) 193–204.
[6] J. Wang, M. Weyland, I. Bikmukhametov, M.K. Miller, P.D. Hodgson, I. Timokhina, Scr. Comput. Sci. Appl. Math. Mater. 160 (2019) 53–57.
[7] F. Danoix, T. Epicier, F. Vurpillot, D. Blavette, J. Mater. Sci. 47 (2012) 1567–1571.
[8] T. Furuhara, Y. Zhang, M. Sato, G. Miyamoto, M. Enoki, H. Ohtani, T. Uesugi, H. Numakura, Scr. Comput. Sci. Appl. Math. Mater. 223 (2023), 115063.
[9] S. Taniguchi, G. Shigesato, M. Sugiyama, ISIJ Int. 62 (2022) 984–991.
[10] R.G. Baker, J. Nutting, ISI Spec. Rep. 64 (1959) 1.
[11] C. Ioannidou, A. Navarro-López, A. Rijkenberg, R.M. Dalgliesh, S. Koelling, C. Pappas, J. Sietsma, A.A. van Well, S.E. Offerman, Acta Mater. 201 (2020) 217–230.
[12] R. Shi, Y. Ma, Z. Wang, L. Gao, X.-S. Yang, L. Qiao, X. Pang, Acta Mater. 200 (2020) 686–698.
[13] A.P. Thompson, H. M. Aktulga, R. Berger, D.S. Bolintineanu, W. M. Brown, P.S. Crozier, P.J. in 't Veld, A. Kohlmeyer, S.G. Moore, T.D. Nguyen, R. Shan, M.J. Stevens, J. Tranchida, C. Trott, S.J. Plimpton, *Comput. Phys. Commun.* 271 (2022) 108171.
[14] M. Volmer, A. Weber, Z. Phys. Chem. 119 (1926) 277–301.
[15] R. Becker, W. Döring, Annalen der Physik 416 (1935) 719–752.
[16] R. Kampmann, R. Wagner, Decomposition of Alloys: The Early Stages, Pergamon Press, 1984, pp. 91–103.
[17] M. Perez, M. Dumont, D. Acevedo-Reyes, Acta Mater. 56 (2008) 2119.
[18] R.J. Slooter, M.H.F. Sluiter, W.G.T. Kranendonk, C. Bos, in preparation.
[19] H.-K. Kim, W.-S. Jung, B.-J. Lee, J. Mater. Res. 25 (7) (2010) 1288–1297.
[20] H.-K. Kim, W.-S. Jung, B.-J. Lee, Acta Mater. 57 (2009) 3140–3147.
[21] G. Kresse, J. Hafner, Phys. Rev. B 47 (1993) 558(R).
[22] G. Kresse, J. Hafner, Phys. Rev. B 49 (1994) 14251–14269.
[23] G. Kresse, J. Furthmüller, Comput. Mater. Sci. 6 (1996) 15–50.
[24] G. Kresse, J. Furthmüller, Phys. Rev. B 54 (1996) 11169–11186.
[25] G. Kresse, D. Joubert, Phys. Rev. 59 (1999) 1758.
[26] H. Jonsson, G. Mills, K.W. Jacobsen, Classical and Quantum Dynamics in Condensed Phase Systems, World Scientific, 1998.
[27] H. Sawada, S. Taniguchi, K. Kawakami, T. Ozaki, Model. Simul. Mater. Sci. Eng. 21 (2013), 045012.
[28] H. Sawada, S. Taniguchi, K. Kawakami, T. Ozaki, Metals 7 (2017) 277–289.
[29] D. Simonovic, C.K. Ande, A.I. Duff, F. Syahputra, M.H.F. Sluiter, Phys. Rev. B 81 (2010), 054116.
[30] N.W. Ashcroft, N.D. Mermin, Solid State Physics, Brooks/Cole, Belmont, CA, USA, 1976.
[31] C.K. Ande, M.H.F. Sluiter, Metal. Mater. Trans. A 43 (2012) 4436–4444.
[32] A.M. Sherman, G.T. Eldis, M. Cohen, Metall. Trans. A 14 (1983) 995–1005.
[33] K.A. Taylor, G.B. Olson, M. Cohen, J.B. van der Sande, Metall. Trans. A 20 (1989) 2749–2765.
[34] R. Rementeria, C. Capdevila, R. Domínguez-Reyes, J.D. Poplawsky, W. Guo, E. Urones-Garrote, C. Garcia-Mateo, F.G. Caballero, Metall. Mater. Trans. A 49A (2018) 5277–5287.
[35] S. Allain, F. Danoix, M. Goune, K. Hoummada, D. Mangelinck, Phil. Mag. Lett. 93 (2013) 68–76.

[36] P. Maugis, F. Danoix, M. Dumont, S. Curelea, S. Cazottes, H. Zapolsky, M. Gouné, Mater. Lett. 214 (2018) 213–216.
[37] S. Chentouf, S. Cazottes, F. Danoix, M. Gouné, H. Zapolsky, P. Maugis, Intermetallics 89 (2017) 92–99.
[38] D. Kandaskalov, P. Maugis, Comput. Mater. Sci. 126 (2017) 278–296.
[39] D. Kandaskalov, P. Maugis, Comput. Mater. Sci. 150 (2018) 524–534.
[40] J. Xu, C.T. Liu, M.K. Miller, H. Chen, Phys. Rev. B 79 (2009) 020204(R).
[41] B.-J. Lee, Acta Mater. 54 (2006) 701–711.
[42] C.D. Versteylen, N.H. van Dijk, M.H.F. Sluiter, Phys. Rev. B 96 (2017), 094105.
[43] C. Hin, Y. Bréchet, P. Maugis, F. Soisson, Acta Mater. 56 (2008) 5653–5667.
[44] C. Hin, Y. Bréchet, P. Maugis, F. Soisson, Acta Mater. 56 (2008) 5535–5543.
[45] Supplementary data available at https://doi.org/10.1016/j.commatsci.2023.112455.
[46] M.H.F. Sluiter, Mater. Res. Soc. Symp. Proc. 979 (2006) 1403.
[47] T. Klymko, M.H.F. Sluiter, J. Mater. Sci. 47 (2012) 7601–7614.
[48] X.-W. Lei, D.-Y. Li, X.-H. Zhang, T.-X. Liang, Metall. Mater. Trans. A 50 (2019) 2978–2990.
[49] M.K. Kang, Y.Q. Yang, Q.M. Wei, W.M. Yang, X.K. Meng, Metall. Mater. Trans. A 25 (1994) 1941–1946.
[50] X.K. Wu, X.Y. Zhang, X.K. Meng, M.K. Kang, Y.Q. Yang, Mater. Lett. 22 (1995) 141–144.
[51] Q. Luo, M. Kitchen, S. Abubakri, Metals 7 (2017) 258.